PHYSICAL REVIEW B VOLUME 51, NUMBER 19 15 MAY 1995-I

Detailed microscopic calculation of phonon-mediated electron-electron scattering in aluminum

A. Jaquier, R. Stubi, P.-A. Probst, and R. Huguenin
Institut de Physique Experimentale, Universite de Lausanne, 1015 Lausanne-Dorigny, Switzerland

W. E. Lawrence
Department of Physics, Dartmouth College, Hanover, New Hampshire 03755

(Received 6 December 1994)

The phonon-mediated electron-electron scattering rate has been calculated in Al using a realistic band structure and phonon spectrum. The electron-phonon contribution has also been calculated as an extension of previous calculations to provide a detailed Fermi-surface map and special orbit averages for comparison with experiment. Comparison with recent radio-frequency size-effect data in which the two contributions are resolved on three orbits yields agreement in both magnitude and anisotropy for both contributions. The calculated electron-electron scattering rate at points exhibits surprisingly large anisotropy (up to an order of magnitude), which is masked in part by orbit averaging but which could, in principle, be measured experimentally. We argue that the Coulomb interaction, whose contribution is known to be much smaller in Al, is also much less anisotropic. Therefore, an anisotropic T^2 contribution to the scattering rate persisting to low temperatures should be, at least in the simple metals, a signature of the phonon-mediated scattering mechanism.

I. INTRODUCTION

Electron-electron scattering has been seen for a long time in transition metals,[1] but only relatively recently in simple metals, where precise measurements must be made at lower temperatures in order to resolve the T^2 signature obscured at higher temperatures by electron-phonon scattering. The latter has a more rapid temperature dependence, generally resembling T^3 in the quasiparticle scattering rate and T^5 in the electrical resistivity, but often showing complications due to umklapp scattering, Fermi-surface distortion, and phonon dispersion (as we shall discuss with specific examples later).

Electrical resistivity measurements in Al (Refs. 2 and 3) extending down to 1.18 K have been found consistent with a sum of electron-electron and electron-phonon contributions, but existing quasiparticle experiments had failed to resolve a distinct T^2 component (two experiments[4,5] found a T^3 dependence, while Parsons and Steele[6] reported T^n with n varying between 2.2 and 3). In order to resolve this situation, we recently undertook radio-frequency size-effect (RFSE) experiments (reported elsewhere[7]), in addition to the calculation reported here. We were able to resolve both electron-electron and electron-phonon contributions experimentally on three different Fermi-surface orbits. Both contributions are in agreement with orbitally averaged rates computed here, and they are also consistent with the electrical resistivity data.

A further motivation for the present work is that a microscopic calculation of phonon-mediated electron-electron scattering on a distorted Fermi surface has not yet been done. Fully microscopic calculations have been done in the alkali metals Na, K, Rb, and Cs,[8] for the electrical and thermal resistivities involving both Coulomb and phonon-mediated scattering. Approximate calculations for both mechanisms based on a Fermi-liquid parametrization were done for Al, Pb, and the noble metals.[9] MacDonald's approximate calculation for Al is in good agreement (within theoretical and experimental uncertainties) with the electrical resistivity data. A microscopic calculation of the (anisotropic) Coulomb scattering rate was performed for W.[10] The phonon-mediated contribution has not been considered in a similar manner, although a more recent approximate calculation[11] finds phonon-mediated scattering rates in reasonable agreement with experiment in six transition metals (Mo, W, Nb, Ru, Os, and Re) and in Cd. The present microscopic calculation for Al is needed not only to test the validity of the approximate calculations, but also to examine the anisotropy (which is very difficult to estimate within the approximate approaches), and to provide orbit averages which are measured experimentally.

The microscopic underpinnings of the calculation, including the electron wave functions and Fermi surface, the phonon spectra, and resulting electron-phonon interaction needed to compute the scattering rates, are described in Sec. II. In Sec. III we discuss a useful method developed for computing the multiple Fermi-surface integrals encountered with electron-electron scattering. Calculated results are presented in Sec. IV; these include detailed Fermi-surface maps of the scattering rates, as well as orbit and Fermi-surface averages for comparison with experiment. Conclusions are summarized in Sec. V.

II. MICROSCOPIC TREATMENT

Let us begin by summarizing the quasiparticle properties of interest arising from the electron-phonon interaction. The renormalization of quasiparticle velocity at a point on the Fermi surface (effective mass enhancement) is described by the parameter $\lambda(\mathbf{k})$ or $Z(\mathbf{k})$ through

0163-1829/95/51(19)/13005(10)/$06.00

$$\mathbf{v}^{(\mathrm{ren})}(\mathbf{k})=\mathbf{v}(\mathbf{k})/[1+\lambda(\mathbf{k})]=\mathbf{v}(\mathbf{k})/Z(\mathbf{k})\ , \tag{1}$$

where the unlabeled $\mathbf{v}$ is that given by any (effectively one-electron) band calculation. The function $\lambda(\mathbf{k})$ is given by the Fermi-surface integral

$$\lambda(\mathbf{k})=\frac{2}{(2\pi)^3}\int\frac{dS(\mathbf{k}')}{|\mathbf{v}(\mathbf{k}')|}\sum_\sigma\frac{|g_\sigma(\mathbf{k}',\mathbf{k})|^2}{\omega_\sigma(\mathbf{k}'-\mathbf{k})}\ , \tag{2}$$

where

$$g_\sigma(\mathbf{k}',\mathbf{k})=\frac{\hat{\epsilon}_\sigma(\mathbf{k}'-\mathbf{k})\cdot\langle\mathbf{k}'|\nabla V|\mathbf{k}\rangle}{[2\rho\omega_\sigma(\mathbf{k}'-\mathbf{k})]^{1/2}} \tag{3}$$

is the matrix element for scattering an electron from $\mathbf{k}$ to $\mathbf{k}'$ with the absorption of a phonon with wave vector $\mathbf{k}'-\mathbf{k}$ (reduced to the first zone), frequency $\omega_\sigma(\mathbf{k}'-\mathbf{k})$, and polarization $\hat{\epsilon}_\sigma(\mathbf{k}'-\mathbf{k})$; V is the electron-ion pseudopotential; and $dS(\mathbf{k}')$ is a Fermi-surface element at $\mathbf{k}'$. The matrix element for the corresponding phonon emission process is $g^*_\sigma(\mathbf{k}',\mathbf{k})$.

The quasiparticle lifetime suffers from both electron-phonon scattering, which refers to the emission and absorption of real phonons, and from electron-electron scattering, due to the combination of virtual phonon mediation and the Coulomb interaction. The electron-phonon scattering rate for a quasiparticle in a state $\mathbf{k}$ on the Fermi surface is[12]

$$\tau^{-1}_{e\phi}(\mathbf{k})=\frac{4\pi}{(2\pi)^3Z(\mathbf{k})}\int\frac{dS(\mathbf{k}')}{|\mathbf{v}(\mathbf{k}')|}\sum_\sigma\frac{|g_\sigma(\mathbf{k}',\mathbf{k})|^2}{\sinh[\omega_\sigma(\mathbf{k}'-\mathbf{k})/T]}\ , \tag{4}$$

where the temperature T and other quantities are measured in units where $\hbar=k_B=1$. The corresponding electron-electron scattering rate[11] at $\mathbf{k}$ is an integral over three (other) states lying on the Fermi surface, only two of which are independent, the third $(\mathbf{p}+\mathbf{q})$ fixed by crystal momentum conservation as pictured in Fig. 1:

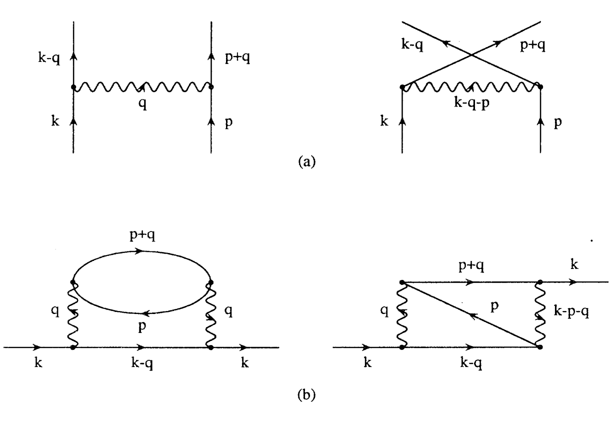

FIG. 1. Feynman diagrams representing the electron-electron interaction (a) as it is written in Eqs. (5)–(7). Equations (5) and (6) may be derived from the imaginary parts of the effective self-energy diagrams (b).

$$\tau^{-1}_{\mathrm{ee}}(\mathbf{k})=\frac{T^2}{(2\pi)^3Z(\mathbf{k})}\times\int\frac{dS(\mathbf{k}-\mathbf{q})}{|\mathbf{v}(\mathbf{k}-\mathbf{q})|}\times\int\frac{dS(\mathbf{p})}{|\mathbf{v}(\mathbf{p})|}\delta[\varepsilon(\mathbf{p}+\mathbf{q})-\varepsilon_F]\Gamma(\mathbf{k},\mathbf{p};\mathbf{q})\ . \tag{5}$$

The δ function keeps $\mathbf{p}+\mathbf{q}$ on the Fermi surface. In fact two of the three quasiparticle *energies* are independent (like the crystal momenta), but these have been integrated to give the prefactor T^2 (the small energy range involved effectively constrains the crystal momenta to the Fermi surface). Equation (5) is equivalent to Eqs. (4) and (5) of Schwartzman and Lawrence,[11] with

$$\Gamma(\mathbf{k},\mathbf{p};\mathbf{q})=V_{\mathrm{ee}}(\mathbf{k},\mathbf{p};\mathbf{q})[V_{\mathrm{ee}}(\mathbf{k},\mathbf{p};\mathbf{q})-\tfrac{1}{2}V_{\mathrm{ee}}(\mathbf{k},\mathbf{p};\mathbf{k}-\mathbf{p}-\mathbf{q})]\ , \tag{6}$$

representing the square of the antisymmetrized two-body matrix element, averaged over initial spin states, of the effective electron-electron interaction pictured in Fig 1:

$$V_{\mathrm{ee}}(\mathbf{k},\mathbf{p};\mathbf{q})=-\sum_\sigma g^*_\sigma(\mathbf{k}-\mathbf{q},\mathbf{k})\omega^{-1}_\sigma(\mathbf{q})g_\sigma(\mathbf{p}+\mathbf{q},\mathbf{p})+\langle\mathbf{k}-\mathbf{q},\mathbf{p}+\mathbf{q}|V_c|\mathbf{k},\mathbf{p}\rangle\ . \tag{7}$$

The first term in Eq. (7) is from virtual phonon mediation in the static limit ($\omega\ll\omega_D$ or $T\ll\Theta_D$), where the phonon propagator becomes independent of electron energy transfer ω and reduces to the inverse of the phonon frequency. It is only in this potential scattering limit that the phonon-mediated interaction contributes as T^2 in Eq. (5) (Ref. 13) (in Al, electron-electron scattering can only be detected experimentally in this regime). The second term in Eq. (7) is just the unsymmetrized (or direct) part of the Coulomb scattering amplitude. The wavy line in Fig. 1 in general represents the sum of these two terms,[13] although in Al the Coulomb contribution to the scattering rate or resistivity has been shown to be less than 10% of the phonon-mediated contribution.[9] Therefore in this work we are primarily interested in the latter, except for a brief mention of the Coulomb contribution in Sec. IV for the sake of comparison.

In computing the scattering rates and mass enhancement we employ the same basic ingredients as Meador and Lawrence,[14] and introduce a couple of minor refinements. The electronic parameters (namely, the Fermi-surface shape, the band velocities, and the wave functions) are obtained from a 4-OPW (orthogonalized plane wave) fit to more recent de Haas–van Alphen areas,[15] whose improved precision makes only minor changes in our computed results. The phonon spectrum is determined from a Born–von Karman fit to neutron data.[16] The electron-phonon interaction is calculated from these ingredients without any further adjustable parameters. The electron-ion form factor which enters the electron-phonon interaction could in principle be considered adjustable, since the Fermi-surface fit determines its values only at the reciprocal-lattice points [111] and [200]. We follow the spirit of Meador and Lawrence,[14] however, in choosing a simple plausible functional form consistent with this fit. They chose the Ashcroft form,[17] which has a single parameter (the atomic core radius) and works well in simple metals generally. In the case of Al, it fits both pseudopotential coefficients reasonably well, but of course not exactly. Because the electron-phonon interaction is quite sensitive to the form-factor values near these points, we prefer to adopt a two-parameter form factor that reproduces both coefficients precisely, while otherwise distorting the Ashcroft form as little as possible. Perhaps the least arbitrary way to do this is to convolute the Ashcroft form with a Gaussian. Physically this smooths out the step at the core radius. In momentum space, it weakens the form factor at the largest momentum transfers, near $2k_F$. We have repeated the calculations of Ref. 14, and find the electron-phonon-scattering rate substantially unchanged. The mass enhancement parameter, which depends more strongly on large-angle scattering, is reduced by somewhat less than 20% while retaining its general anisotropic form. A more detailed comparison is given in Sec. IV.

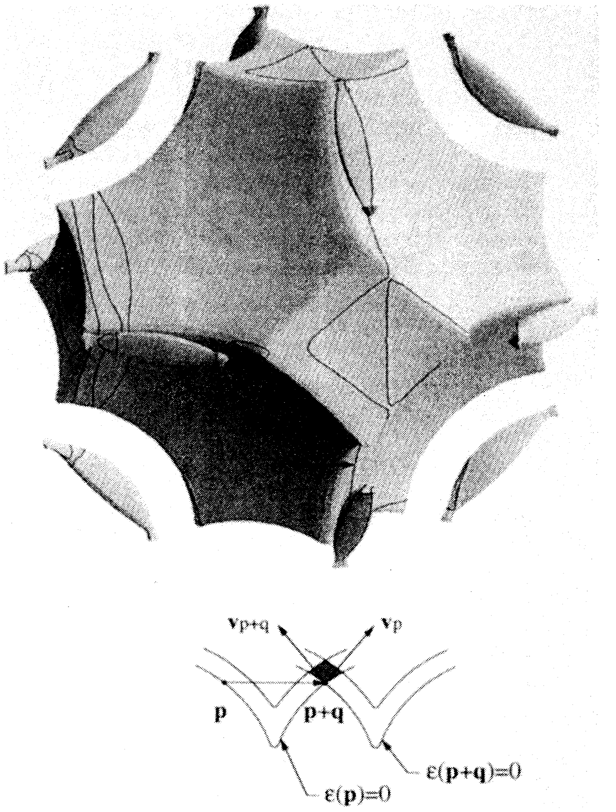

FIG. 2. Contour of the intersection between the original Fermi surface (shown) and an identical Fermi surface displaced through **q** (not shown).

III. EVALUATION OF SURFACE INTEGRALS

Here we discuss the technique used to compute the surface integrals required for τ_{ee}^{-1} in Eq. (5). First note that for each **q** in the first surface integral, we may interpret the remaining integration

$$\int \frac{dS(\mathbf{p})}{|\mathbf{v}(\mathbf{p})|}\delta[\varepsilon(\mathbf{p}+\mathbf{q})-\varepsilon_F] = \int d^3p\,\delta[\varepsilon(\mathbf{p})-\varepsilon_F]\delta[\varepsilon(\mathbf{p}+\mathbf{q})-\varepsilon_F] \tag{8}$$

as the line integral over the intersection of two identical Fermi surfaces, one centered at the origin and the other centered at **q**. This intersection contour is shown for Al in Fig. 2. Physically, the contour represents final states $(\mathbf{p}+\mathbf{q})$ on the Fermi surface shown, and initial states $(\mathbf{p})$ on the displaced Fermi surface (not shown). For Al the contour is always multiply connected, and the Fermi surface may be drawn in an appropriate reduced zone so that the contour is always closed (in contrast, open contours may occur, for example, on the noble-metal Fermi surfaces, depending on **q**). It is apparent that all possible electron-electron scattering events (normal and umklapp if these designations are meaningful) are counted, because for each **q** in the Fermi surface integration (over $\mathbf{k}-\mathbf{q}$), the integration contour is uniquely defined. It is immaterial whether or not **q** lies in the first Brillouin zone so long as all sheets of the Fermi surface appear in the zone where $\mathbf{p}+\mathbf{q}$ resides. Throughout this work, for definiteness, we regard all contour integrals as functions of **q** remapped to the first Brillouin zone.

To remove the δ functions and write the contour integral of Eq. (8) explicitly, we let dp denote a line element along the contour, and $d^2p_\perp$ the area element in the plane locally perpendicular to it. The energy arguments in the δ functions may then be rewritten in the neighborhood of any point **p** on the contour as $\mathbf{v}(\mathbf{p})\cdot\Delta\mathbf{p}_\perp$ and $\mathbf{v}(\mathbf{p}+\mathbf{q})\cdot\Delta\mathbf{p}_\perp$, where $\Delta\mathbf{p}_\perp$ is a vector originating on the contour and lying in the aforementioned plane, and the two velocity vectors are shown in the inset of Fig. 2. It can be shown that

$$\int d^2p_\perp\delta[\varepsilon(\mathbf{p})-\varepsilon_F]\delta[\varepsilon(\mathbf{p}+\mathbf{q})-\varepsilon_F]=|\mathbf{v}(\mathbf{p})\times\mathbf{v}(\mathbf{p}+\mathbf{q})|^{-1}\ , \tag{9}$$

and so Eq. (5) takes the form

$$\tau_{\mathrm{ee}}^{-1}(\mathbf{k})=\frac{T^2}{(2\pi)^3Z(\mathbf{k})}\int\frac{dS(\mathbf{k}-\mathbf{q})}{|\mathbf{v}(\mathbf{k}-\mathbf{q})|} \times\oint_{C(\mathbf{q})}\frac{dp\,\Gamma(\mathbf{k},\mathbf{p};\mathbf{q})}{|\mathbf{v}(\mathbf{p})\times\mathbf{v}(\mathbf{p}+\mathbf{q})|}\ , \tag{10}$$

where the contour $C(\mathbf{q})$ is defined completely by **q**, as described above.

To actually find the contour, we evaluate the secular determinant defining the displaced Fermi surface, $D(\mathbf{p}+\mathbf{q})$, and locate its zeros (by interpolation) along lines joining mesh points **p** on the *original* Fermi surface. These zeros then establish the contour integration mesh.

In general one must compute the contour integral separately for each **k** *and* for each **q** associated with the Fermi-surface integral. The computation may be shortened considerably for the *direct* part of the phonon-mediated interaction, which may be written[18] as the sum of terms in which $\mathbf{k}$ and $\mathbf{p}$ dependences factorize, removing $\mathbf{k}$ dependences from the contour integrals. Since this contribution accounts for more than 90% of the total electron-electron scattering rate in Al, and since furthermore the contour method provides useful checks on the full calculation, it is worth presenting the simplified form. If the phonon-mediated part of (7) is substituted into (6), then the direct part [i.e., the first term of (6)] is

$$\Gamma_d(\mathbf{k},\mathbf{p};\mathbf{q}) = \left[\sum_{\sigma} g_\sigma(\mathbf{k}-\mathbf{q},\mathbf{k})\,\omega_\sigma^{-1}(\mathbf{q})\,g_\sigma(\mathbf{p}+\mathbf{q},\mathbf{p})\right]^2 = \sum_{\sigma,\sigma'} \frac{g_\sigma(\mathbf{k}-\mathbf{q},\mathbf{k})\,g_{\sigma'}(\mathbf{k}-\mathbf{q},\mathbf{k})}{\omega_\sigma(\mathbf{q})\,\omega_{\sigma'}(\mathbf{q})} \times g_\sigma(\mathbf{p}+\mathbf{q},\mathbf{p})\,g_{\sigma'}(\mathbf{p}+\mathbf{q},\mathbf{p})\ , \qquad (11)$$

and the corresponding contribution to the scattering rate is

$$\tau_d^{-1}(\mathbf{k}) = \frac{T^2}{(2\pi)^3 Z(\mathbf{k})} \int \frac{dS(\mathbf{k}-\mathbf{q})}{|\mathbf{v}(\mathbf{k}-\mathbf{q})|} \sum_{\sigma,\sigma'} \left[\frac{g_\sigma(\mathbf{k}-\mathbf{q},\mathbf{k})\,g_{\sigma'}(\mathbf{k}-\mathbf{q},\mathbf{k})}{\omega_\sigma(\mathbf{q})\,\omega_{\sigma'}(\mathbf{q})}\right] M_{\sigma\sigma'}(\mathbf{q})\ , \qquad (12)$$

where the contour integral matrix

$$M_{\sigma\sigma'}(\mathbf{q}) = \oint_{C(\mathbf{q})} dp \left[\frac{g_\sigma(\mathbf{p}+\mathbf{q},\mathbf{p})\,g_{\sigma'}(\mathbf{p}+\mathbf{q},\mathbf{p})}{|\mathbf{v}(\mathbf{p})\times\mathbf{v}(\mathbf{p}+\mathbf{q})|}\right] \qquad (13)$$

depends only on $\mathbf{q}$. Clearly this matrix has the properties

$$M_{\sigma\sigma'}(\mathbf{q}) = M_{\sigma\sigma'}(\mathbf{R}\mathbf{q}) = M_{\sigma'\sigma}(\mathbf{q})\ , \qquad (14)$$

so that all necessary information is contained in six elements of M as functions of $\mathbf{q}$, with $\mathbf{q}$ restricted to the $\frac{1}{48}$th symmetry element of the Brillouin zone ($\mathbf{R}$ is any element of the cubic group). Given these six functions, $\tau_d^{-1}(\mathbf{k})$ may be computed for every $\mathbf{k}$ as a single Fermi-surface integral. This simplified form is therefore convenient for producing a detailed Fermi-surface mapping of $\tau_d^{-1}(\mathbf{k})$, and may also be used as a check on the more lengthy computations required for the exchange contribution to $\tau_{ee}^{-1}(\mathbf{k})$.

A further simplification occurs for the Fermi-surface average,

$$\tau_d^{-1} = \langle \tau_d^{-1}(\mathbf{k}) \rangle_{\mathrm{FS}} = \frac{1}{(2\pi)^3 N_0 Z} \int \frac{dS(\mathbf{k})}{|\mathbf{v}(\mathbf{k})|} \tau_d^{-1}(\mathbf{k})\ , \qquad (15)$$

where N_0 is the density of states per spin at the Fermi level. Substitution of (12) into (15) presents a double Fermi-surface integral which may be rewritten as

$$\int \frac{dS(\mathbf{k})}{|\mathbf{v}(\mathbf{k})|} \int \frac{dS(\mathbf{k}-\mathbf{q})}{|\mathbf{v}(\mathbf{k}-\mathbf{q})|} = \int d^3k \int d^3q\ \delta[\varepsilon(\mathbf{k})-\varepsilon_F]\,\delta[\varepsilon(\mathbf{k}-\mathbf{q})-\varepsilon_F]\ .$$

Changing the order of integrations, we see that the $\mathbf{k}$ integral of the two δ functions reduces to a contour integral (dk) involving the explicit vertex functions in Eq. (12) and the denominator $|\mathbf{v}(\mathbf{k})\times\mathbf{v}(\mathbf{k}-\mathbf{q})|$. Equations (12) and (15) thus lead to

$$\tau_d^{-1} = \frac{T^2}{(2\pi)^6 N_0 Z} \int_{\mathrm{BZ}} d^3q \sum_{\sigma,\sigma'} \frac{M_{\sigma\sigma'}^2(\mathbf{q})}{\omega_\sigma(\mathbf{q})\,\omega_{\sigma'}(\mathbf{q})}\ , \qquad (16)$$

where the $\mathbf{q}$ integration is restricted to the first Brillouin zone so that each scattering event is counted once (and only once), according to the definition of the contour integral as described following Eq. (8). The summand in Eq. (16) may be written as $\mathrm{Tr}\,U^2(\mathbf{q})$,[11] where U is the matrix defined by $U_{\sigma\sigma'} = M_{\sigma\sigma'}(\omega_\sigma\omega_{\sigma'})^{-1/2}$.

IV. FERMI-SURFACE MAPS OF SCATTERING RATES

The computed Fermi surface is shown in Fig. 3, with special points identified. We have computed the scattering rates over the entire Fermi surface, except for the electron-electron exchange term which, because it is much more time consuming, was computed only at selected points. Since we will compare with experimental data that measure energy averages of scattering rates, we will present our theoretical results in the same form. The energy-averaged scattering rate is

$$\langle \tau^{-1}(\mathbf{k}) \rangle_\varepsilon = \int d\varepsilon(-\partial f/\partial\varepsilon)\,\tau^{-1}(\hat{k},\varepsilon) = A\,\tau^{-1}(\mathbf{k})\ , \qquad (17)$$

where $\tau^{-1}(\mathbf{k}) = \tau^{-1}(\hat{k},\varepsilon=0)$ is the value of the Fermi sur-

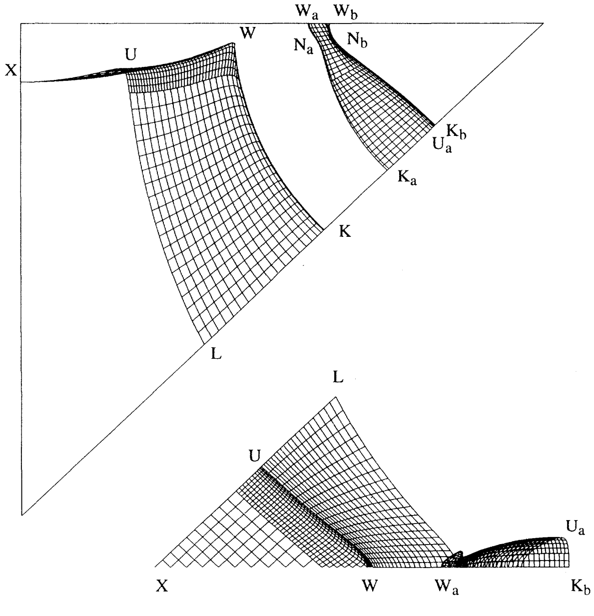

FIG. 3. Minimum symmetry element of the Fermi surface showing integration mesh and identifying special points. Two perspectives are shown.

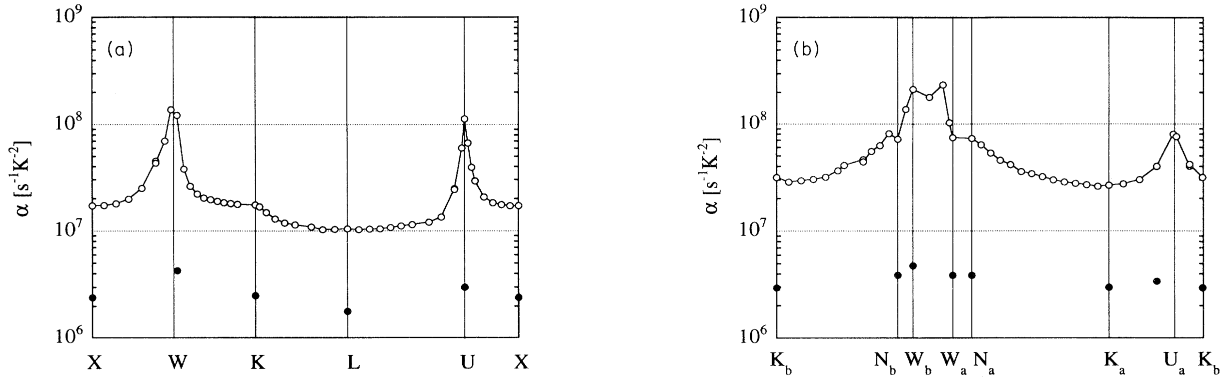

FIG. 4. Phonon-mediated electron-electron scattering rate $\alpha=\tau_{ee}^{-1}T^{-2}$ on the border of the minimum symmetry element of the (a) second- and (b) third-zone Fermi-surface sheet.

face, and A is only weakly temperature dependent, taking the values $\frac{4}{3}$ for electron-electron scattering and $\frac{12}{7}$ for electron-phonon scattering when the power laws T^2 and T^3 apply, for example.

Consider first the phonon-mediated electron-electron contribution. Figures 4(a) and 4(b) show the T^2 coefficient $\alpha=\langle\tau_{ee}^{-1}\rangle_\varepsilon/T^2$ (as a continuous curve for the direct contribution and at selected points for the exchange contribution), on the border of the minimum symmetry element for the second and third zones of the Fermi surface. Note that the exchange term is never more than $\frac{1}{6}$ of the direct term (point L) and follows the same trend but with much less anisotropy (for example it is only $\frac{1}{25}$ of direct term at point W). Particular point values (direct, exchange, and total) are reported in Table I. The minimum values of the coefficient α_{tot} occur at the

TABLE I. Calculated scattering rate parameters $\alpha=\tau_{ee}^{-1}T^{-2}$ and $\beta=\tau_{e\phi}^{-1}T^{-3}$ and renormalization parameter λ at points of interest on the Fermi surface. Also shown are orbit averages for the three orbits measured in Ref. 7 (see Table II), and three surface averages.

Location	α_{direct} (10^7 s^{-1}K^{-2})	$\alpha_{\text{exch.}}$	α_{total}	$\beta(T\to 0)$ (10^7 s^{-1}K^{-3})	$\beta(T=10$ K$)$	λ
points						
L	1.1	0.2	0.9	0.29[a]	0.29[a]	0.31
U	11	0.3	11	1.2	2.7	0.44
X	1.7	0.2	1.5	0.30[a]	0.29[a]	0.35
W	12	0.4	12	4.9	3.5	0.48
K	1.8	0.3	1.5	4.8	2.4	0.44
W_a	7.5	0.4	7.1	9.8	3.2	0.40
W_b	21.5	0.5	21	4.8	3.3	0.48
N_a	7.3	0.4	6.9	11.1	5.0	0.36
N_b	7.2	0.4	6.8	2.5	3.5	0.41
K_a	2.7	0.3	2.4	17.0	6.7	0.31
K_b	3.2	0.3	2.9	0.36	1.9	0.33
U_a	8.0	0.4	7.6	5.5	3.7	0.30
orbital averages[b]						
second zone						
⟨100⟩+6°	2.4	0.2	2.2	0.38	0.59	0.36
third zone						
⟨100⟩	4.1	0.3	3.8	4.1	4.1	0.32
⟨110⟩	4.2	0.3	3.9	4.2	4.1	0.32
surface averages						
second zone	2.5	0.2	2.3	0.78	0.90	0.37
third zone	5.9	0.3	5.6	4.9	4.6	0.33
Fermi surface	3.3	0.3	3.0	1.8	1.8	0.36

[a] Reference 14.

[b] Orbits are defined by normal vectors. The second zone orbit is noncentral.

L points ($\alpha_L = 0.87\times10^7$ $\mathrm{s^{-1}K^{-2}}$), and similar local minima occur at the X points ($1.7\times\alpha_L$). The second-zone maxima ($13-14\times\alpha_L$) occur along the V_{111} ridges surrounding the square faces of the Brillouin zone. These maxima are sharp when crossing the ridge, but almost uniform when moving along it. The saddle points at K on the second-zone V_{200} ridges appear as weak local maxima ($1.7\times\alpha_L$) when crossing that ridge. The absolute Fermi-surface maxima ($24\times\alpha_L$) occur along the junctions of the third-zone arms near the points W_b. Local third-zone minima occur at points K_a and K_b (2.7 and $3.3\times\alpha_L$, respectively). Local maxima (about $9\times\alpha_L$) extend from near the U_a points along the V_{111} ridges until they rise sharply near the junctions.

The phonon-mediated scattering rate, like λ (to be discussed below), receives contributions from large-angle as well as small-angle scattering events. Umklapp processes contribute everywhere but more importantly near zone boundaries, while the multiple-plane-wave character of wave functions produces more localized effects along the ridges. The general trends seen in the anisotropy of τ_{ee}^{-1} are, for the most part, understandable in these terms. However, the sharp maxima found on the narrow V_{111} ridges are unexpected, and despite a long reflection we have no satisfying explanation for them. Also somewhat surprising is the small contribution from the exchange term which could, in principle, be as large as half the direct term.[11] The average Fermi-surface value is in good agreement with previous approximate theoretical calculations by Macdonald[9] and Schwartzman and Lawrence,[11] although larger than both (by about 40% and 90%, respectively). This difference could be considered attributable in part to the smallness of the exchange contribution, which contributes negatively. The anisotropy found here could not have been predicted from these simplified treatments because their approximations involved angular averaging.

We have estimated the purely Coulomb contribution to the scattering rate based upon a simple model for the scattering amplitude between single OPW's which involves a screening length parameter. The effect of the Al band structure is to introduce about 10% anisotropy (independently of the screening length), without changing the average magnitude significantly. Extremal values occur near the zone boundaries, and there is very little difference between the average values on the two zones. We have not attempted to improve upon previous many-body calculations of the underlying scattering amplitude,[19] since this is found to be small in Al.[9]

Figures 5(a) and 5(b) show the T^3 coefficient $\beta = \langle \tau_{e\phi}^{-1} \rangle_\varepsilon / T^3$ of the electron-phonon scattering rate at various temperatures (also see Table I). These are very close to those presented by Meador and Lawrence,[14] but available now on the whole Fermi surface. The maximal anisotropy (50-1, considering the entire Fermi surface) occurs in the low-temperature limit. The lowest values are found in the free-electron-like regions of the second zone (near points L and X) and a less pronounced local minimum occurs near the third-zone point K_b. Maximal values are found on the V_{200} ridges of both zones, and smaller local maxima occur on the V_{111} ridges of both zones. As temperature increases the intrazone anisotropies wash out at different rates: The second-zone anisotropy decreases from 20-1 near $T = 0$ K, to 2-1 at $T = 100$ K (which is $\frac{1}{4}$ of the Debye temperature of Al). The third-zone anisotropy drops more quickly, from 40-1 near $T = 0$ K to 3-1 at $T = 10$ K; then it disappears almost completely as the average value drops, approaching the average second-zone value near $T = 100$ K. Only in the free-electron regions near L and X does theory predict pure T^3 behavior throughout the experimentally accessible temperature range (say, $T < 15$ K). Deviations (increasing β) are predicted above about 15 K near X and 25 K near L. Regarding the Fermi surface as a whole, β tends to increase with temperature in free-electron-like regions, and generally to decrease with temperature near ridges, the more rapid decrease near V_{200} ridges. Figure 6 shows typical calculated point scattering rates for points lying on one of the measured third-zone orbits, together with the calculated orbit average. It is striking that despite the wide variation in temperature dependences seen at individual points, the orbit average has

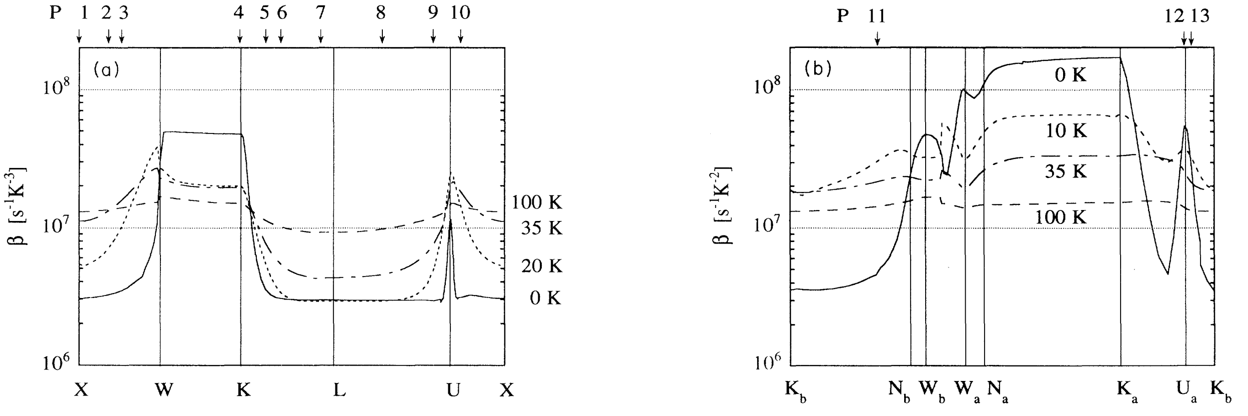

FIG. 5. Electron-phonon scattering rate $\beta = \tau_{e\phi}^{-1} T^{-3}$ on the border of the minimum symmetry element of the (a) second- and (b) third-zone Fermi-surface sheet. Points labeled $P1, P2, \ldots$ identify the available SLLR data shown in Table II.

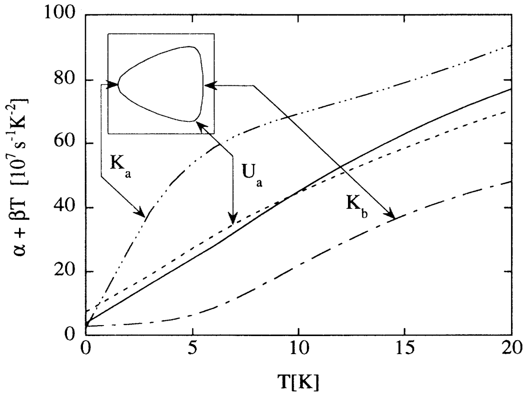

FIG. 6. Total inelastic quasiparticle scattering rate $\alpha+\beta T=\tau^{-1}T^{-2}$ at representative points on the principal (110) orbit of the third zone, compared with the orbit average. Corresponding values of α and β are given in Table I.

nearly cubic dependence over a broader temperature range than do any of the point rates. A similar finding was reported in Ref. 14 on a single orbit, and we find this behavior to be quite typical of orbits on the Al Fermi surface (see Ref. 7 for further discussion). Model calculations exploring the range of temperature dependences that can occur for orbit averages are found in Ref. 20.

Although most of the temperature dependence shown in Figs. 5(a) and 5(b) occurs outside the experimental range for RFSE or surface-Landau-level resonance (SLLR), there are two interesting reasons for discussing it in this much detail. First, similar or greater anisotropy may be present in the transport relaxation rate, which can manifest itself in the form of deviations from Matthiessen's rule in the electrical resistivity (i.e., nonadditivity of the electron-phonon and electron-impurity contributions). This effect is seen at temperatures well above those where RFSE and SLLR are effective. Second, it is instructive (if academic) to note that the anisotropy of $\lambda(\mathbf{k})$ is related to that of the quasiparticle electron-phonon scattering rate by the identity

$$\lim_{T\to\infty} \tau_{e\phi}^{-1}(\mathbf{k})=2\pi T\lambda(\mathbf{k}) , \tag{18}$$

which follows directly from Eqs. (2) and (4). There is a similar identity [Eqs. (41) and (42) of Ref. 21] relating the high-temperature electrical resistivity to a (surface-averaged) transport λ. The identity above is interesting because it holds *pointwise*. It is remarkable that the anisotropies are already quite similar by only 100 K, as shown in Fig. 7. Perhaps the criterion for similar anisotropies is that typical phonon wave vectors need only span the equivalent of a minimum symmetry element, not the whole Fermi surface.

The calculated values of λ are very similar in functional form to those presented by Meador and Lawrence,[14] but lower in magnitude by between 17% and 20%. This is almost entirely the result of using a different form factor, one that matches precisely both pseudopotential coefficients. The calculated Fermi-surface average is also lower than that determined from specific-heat data, namely 0.43,[22] but close to that determined from the superconducting transition temperature, 0.38 (Ref. 23)–0.39 (Ref. 24).

The phonon-mediated electron-electron scattering rate is similarly sensitive to the form factor because it depends on large-angle scattering. The electron-phonon rate, on the other hand, depends on small-angle scattering at low temperatures, where it is quite insensitive to this change.

Recent RFSE measurements,[7] two orders of magnitude more precise than previous ones in Al, have been performed. The experiment allows a clear separation of electron-phonon and electron-electron contributions to the scattering rate by varying experimental conditions on which only the electron-phonon contribution depends. Both contributions are in good overall agreement with our calculations, as seen in Table II. The electron-phonon rates are in excellent agreement, and the measured electron-electron rates are about half the theoretical rates overall, the worst case being the discrepancy of a factor of 3 for the second-zone orbit, which spans both free-electron-like regions and ridges. It is particularly

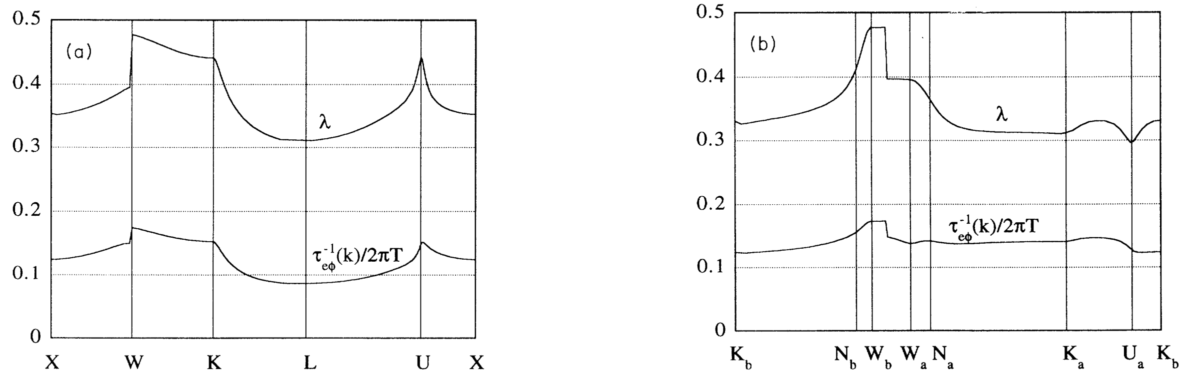

FIG. 7. Anisotropies of $\lambda(\mathbf{k})$ and $\tau_{e\phi}^{-1}(\mathbf{k})$ are compared along the border of the minimum symmetry element of the Fermi surface. The scattering rate is expressed in a dimensionless form whose values should approach $\lambda(\mathbf{k})$ at high temperatures [Eq. (18) of the text]. The anisotropy of $\tau_{e\phi}^{-1}$ is slightly greater than that of λ in the second zone.

gratifying nevertheless that the measured interzone anisotropies agree with theory for both mechanisms. Unfortunately, existing experimental data do not allow a definitive measure of the anisotropy of the electron-electron scattering rate within a single zone, as one would particularly like to confirm the largest predicted values of $\tau_{ee}^{-1}(\mathbf{k})$ occurring on the V_{111} ridges.

In previous RFSE measurements[5,6] on Al, the authors described their data only with single power laws, because of the lack of precision. Perhaps most interesting are the results presented by Parsons and Steele,[6] whose data were obtained using the tilted field effect in the ⟨100⟩ and ⟨111⟩ free-electron-like regions. Our calculated electron-phonon and electron-electron contributions to the scattering rate are comparable in magnitude in the measured temperature range and consistent with the exponents of the best power laws (2.2–2.6) published by the authors.

SLLR measurements,[4] on the other hand, lack sufficient precision to resolve departures from T^3 behavior in the temperature range studied, but they nicely complement the RFSE data in revealing the anisotropy of the electron-phonon scattering rate at points. Meador and Lawrence compared these data with theory at a few calculated points, and we add some further points (Table II) to help fill out the picture. We specify the range of computed β values in those cases where it is broad (these may be read approximately from Fig. 5); otherwise we just state the average value. It should be noted that the experimentally determined values of β would be reduced if T^2 terms (as computed here, for example) were subtracted from the data. This effect is largest near the X and L points, where it produces a decrease of about 20%. Also, the discrepancy between theory and experiment, particularly at points $P4$ and $P5$, may reflect the fact that SLLR measurements average over a finite, if small, arc

TABLE II. A comparison of theoretical and experimental scattering rates for Fermi-surface points (experimental analysis for T^3 only), orbit averages, and the Fermi-surface average related to electrical resistivity ($A=\rho_{ee}/T^2$) Points $P1$, $P2$, etc. are identified in Fig. 5.

Points			β theory (10^7 s^{-1}K^{-3})	β expt.	T range (K)
second zone					
$P1$			0.30[a]	0.41±0.03[b]	4–13
$P2$			0.30–0.38	0.63±0.14[b]	7–11
$P3$			0.34–0.40	1.2±0.3[b]	4–11
$P4$			3.2	1.5±0.7[b]	2–5
$P5$			0.38	1.2±0.3 [b]	4–10
$P6$			0.30	0.35±0.04[b]	4–13
$P7$			0.29[a]	0.39±0.03[b]	4–13
$P8$			0.29	0.54±0.05[b]	4–11
$P9$			0.32	0.71±0.09[b]	4–12
$P10$			0.30–0.60	0.78±0.16[b]	4–10
near ⟨100⟩			0.30	0.25±0.04[c]	4–7
near ⟨111⟩			0.29	0.19±0.02[c]	4–10
third zone					
$P11$			0.8–3.0	2.6±0.3[b]	3–9
$P12$			4.0–4.8	5.0±0.5[b]	2–8
$P13$			3.2	3.1±0.3[b]	2–9
Orbit averages	α theory (10^7 s^{-1}K^{-2})	α expt.			
second zone					
⟨100⟩+6°	2.2	0.68±0.05[d]	0.42	0.54±0.02[d]	0.3–10
third zone					
⟨100⟩	3.8	1.9±0.5[d]	2.4	2.6±0.2[d]	0.8–6
⟨110⟩	3.9	2.6±0.5[d]	2.4	2.6±0.2[d]	1.0–6
FS average (resistivity)	A theory (fΩ m K^{-2})	A expt.			
	5.7	2.7–3.0[e]			1.2–2.2
	5.7	3.7–4.7[f]			2.8–4.2

[a] Reference 14.
[b] Reference 4.
[c] Reference 6.
[d] Reference 7.
[e] Reference 2.
[f] Reference 3.

length on the Fermi surface. Finally, we include in this comparison the results from two limiting-point RFSE orbits studied in Ref. 6. These were fitted to T^3 laws over the indicated temperature ranges.

The global Fermi surface average of the calculated electron-electron scattering rate may be converted into a corresponding electrical resistivity through $\rho_{ee}=4\pi\Delta(1+\lambda)\Omega_p^{-2}\langle\tau_{ee}^{-1}\rangle$ [Eq. (20) of Ref. 11], where brackets denote both Fermi-surface and energy averages, Δ is the umklapp scattering parameter, and Ω_p is the plasma frequency parameter whose square is proportional to the Ferm-surface integral of the electron velocity. Using values quoted in Table IV of Ref. 11 and the value of λ calculated here, we find $\rho_{ee}/T^2=A=5.7$ fΩ m/K^2. The earlier approximate theoretical treatments gave the values $A=4.1$ and 3.0 fΩ m/K^2 (Refs. 9 and 11, respectively). The present value is compared in Table II with the high-resolution measurements on 12 different Al samples by Ribot *et al.*[2] in the temperature range extending from 1.18 to 4.2 K. They found that the data conformed to a sum of T^2 and T^5 contributions from 1.18 up to 2.2 K, but not above. In this interval the T^2 coefficient was found in the range 2.7–3.0 fΩ m/K^2, with the value 2.8 fΩ m/K^2 within the estimated error for every sample. Hou and Kos[2] reanalyzed the same data from nine of the Ribot *et al.* samples, as well as electrical resistivity data on one of their own samples. They found that a sum of constant, T^2 and T^5 terms fit well between 2.85 and 4.2 K, leaving an additional resistivity at low temperatures that could be fit to a Kondo-like temperature dependence. The T^2 coefficients attributed to electron-electron-scattering were in the range $A=3.7$–4.7 fΩ m/K^2 with an average value of 4.14 fΩ m/K^2. A Kondo temperature of 1.6 K was found for all five of the samples for which sufficient low-temperature data exist to determine it. The residual resistivity ρ_0 varied by more than two orders of magnitude (0.66–110 pΩ m) in these samples. The magnetic impurity responsible (if any) is not known, and it is surprising that the Kondo temperature does not vary considering the large variation in ρ_0. It seems to us that electron-electron and electron-phonon scattering provide a sound physical basis for T^2 and T^5 variations in the lower-temperature range, with deviations expected at higher temperatures. In fact, deviations from Matthiessen's rule are evident in the data, and could plausibly arise from the combination of anisotropic electron-phonon and electron-impurity scattering. This would be expected to manifest itself in the onset of a slower-than-T^5 dependence of the electron-phonon contribution with increasing temperature. At sufficiently low temperatures, in contrast, both temperature-dependent contributions saturate and exhibit ρ_0-independent T^2 and T^5 contributions.

It is pleasing to note that the electrical resistivity and RFSE data appear to be consistent with one another regarding the electron-electron mechanism, which resolves a long-standing (apparent) contradiction between the quasiparticle and transport data. In fact the Ribot *et al.* resistivity coefficient A corresponds very closely to the RFSE coefficient α, both being about a factor of 2 below the corresponding theoretical values. It should be remarked in this connection that the theoretical resistivity ρ_{ee} is considerably less certain than the theoretical scattering rates, primarily because of uncertainty in the umklapp parameter Δ, for which realistic microscopic calculations have been carried out only in the alkali metals.[8] Those calculations suggest that in Al, Δ could easily be less than the currently accepted estimate 0.4. A modest correction to this theoretical parameter would not invalidate our conclusions, however.

V. CONCLUSION

Using a 4-OPW pseudopotential fit to the Fermi surface, and a Born–von Karman fit to the phonon spectrum, and adopting the simplest pseudopotential form factor consistent with this, we calculated, without any further adjustable parameters, a complete Fermi-surface map of the phonon-mediated electron-electron scattering rate in Al. To our knowledge, this is the first such microscopic calculation for a distorted Fermi surface. A contour integral method was developed to map out the direct part over the entire Fermi surface and exhibit its surprisingly large anisotropy in detail. The exchange part, computed at a few typical points, is at most $\frac{1}{6}$ of the direct part. We found that the phonon-mediated electron-electron scattering rate depends, like the mass enhancement, on large-angle scattering events as well as short-angle events, in contrast to the electron-phonon scattering rate. We also extended previous calculations of the mass enhancement factor and the electron-phonon scattering rate to cover all the mesh points and provide necessary orbit averages. Finally we estimated the Coulomb contribution, known to be much smaller, and argued that this is much less anisotropic (as expected) than the phonon-mediated contribution.

The calculated orbital averages of both electron-phonon and phonon-mediated electron-electron scattering rates agree with recent high-precision RFSE measurements,[7] which involve a second-zone and two third-zone orbits. The experiments resolve electron-phonon and electron-electron contributions by exploiting the dependence of the former on radio frequency and sample thickness. In agreement with previous calculations,[14] we found sharp deviations from T^3 behavior for point rates, but these tend to average out toward T^3 dependence when computed on all three orbits. Orbit averages also conceal the large intraband anisotropies calculated in point rates from both mechanisms, so that the anisotropy of orbit averages is less than point anisotropies calculated within each band.

The Fermi-surface average of the phonon-mediated electron-electron scattering rate is in good agreement with the value inferred from the electrical resistivity data,[2,3] as it is with previous more approximate theoretical calculations.[9,11] The computed Fermi-surface average of the mass enhancement parameter λ is smaller than the value inferred from specific-heat data, but in reasonable agreement with that inferred from superconductivity.

In summary, with the simplest consistent microscopic theoretical framework, we have shown that we obtain reasonable overall agreement with all pertinent available experimental data. This work shows that anisotropy of a T^2 term in the scattering rate persisting to low temperatures may be a signature of the phonon-mediated electron-electron mechanism in the simple metals. Further experimental data could confirm the extreme anisotropy which we predict on all the V_{111} ridges. Further theoretical work might also be useful in providing insight into the general origin of this anisotropy.

---

[1] V. A. Gasaparov and R. Huguenin, Adv. Phys. **42**, 393 (1993).

[2] J. H. J. M. Ribot, J. Bass, H. Van Kempen, R. J. M. Van Vucht, and P. Wyder, J. Phys. F **9**, L117 (1979); Phys. Rev. B **23**, 532 (1981).

[3] Y. Z. Hou and J. F. Kos, J. Phys. Condens. Matter **5**, 7797 (1993).

[4] T. Wegehaupt and R. E. Doezema, Phys. Rev. B **18**, 742 (1978).

[5] V. A. Gasparov and M. H. Harutunian, Solid State Commun. **19**, 189 (1976).

[6] D. Parsons and C. A. Steel, J. Phys. F **9**, 1783 (1979).

[7] A. Jaquier *et al.*, J. Phys. Condens. Matter **6**, 11 081 (1994).

[8] A. H. MacDonald, R. Taylor, and D. J. W. Geldart, Phys. Rev. B **23**, 2718 (1981).

[9] A. H. MacDonald, Phys. Rev. Lett. **44**, 489 (1980).

[10] C. Potter and G. J. Morgan, J. Phys. F **9**, 493 (1979).

[11] K. Schwartzamn and W. E. Lawrence, Phys. Rev. B **48**, 14 089 (1993).

[12] See, for example, Eq. (2.24) of D. K. Wagner and R. Bowers, Adv. Phys. **27**, 651 (1978).

[13] K. Schwartzman and W. E. Lawrence, Phys. Rev. B **37**, 1136 (1988).

[14] A. B. Meador and W. E. Lawrence, Phys. Rev. B **15**, 1850 (1977).

[15] W. Joss and R. Monnier, J. Phys. F **10**, 9 (1980).

[16] W. M. Hartmann and T. O. Milbrodt, Phys. Rev. B **3**, 4133 (1971).

[17] N. W. Ashcroft, Phys. Lett. **23**, 48 (1966). We have used the precise form quoted in Eq. (2) of N. W. Ashcroft and W. E. Lawrence, Phys. Rev. **175**, 938 (1968).

[18] See the Appendix of Ref. 13.

[19] A. H. MacDonald and D. J. W. Geldart, J. Phys. F **10**, 677 (1980).

[20] W. E. Lawrence, J. Phys. Condens. Matter **5**, 679 (1993).

[21] P. B. Allen, Phys. Rev. B **17**, 3725 (1978).

[22] P. B. Allen, Phys. Rev. B **36**, 2920 (1987).

[23] W. L. McMillan, Phys. Rev. **167**, 331 (1968).

[24] J. W. Garland and P. B. Allen, Physica **55**, 669 (1971).

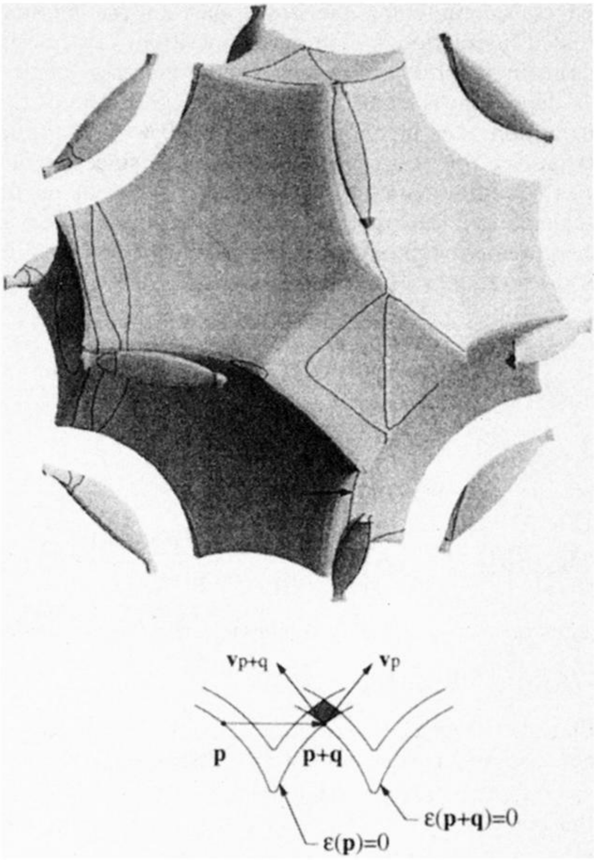

FIG. 2. Contour of the intersection between the original Fermi surface (shown) and an identical Fermi surface displaced through **q** (not shown).